Supporting information

Carbon-Tetrel bond, cooperative existence and disappearance in elastically bendable fluorescent organic single crystals by operating within the hierarchy of non-covalent interactions

Sumy Joseph[a*], Shilpa Munthikkot[a], Velluvakandi Chaluvalappil Saheer[b] and Srinu Tothadi[c]

[a] Postgraduate and Research Department of Chemistry, Nirmalagiri College, Affiliated to Kannur University, Kannur, Kerala, 670701, India.
[b] Department of Chemistry, Government Brennen College, Affiliated to Kannur University, Thalassery, Kerala, 670106, India.
[c] Marine Elements and Marine Environment Division (MEMED), CSIR-Central Salt & Marine Chemicals Research Institute (CSMCRI), Gijubhai Badheka Marg, Bhavnagar-364002 India.

1. PROTON AND CARBON NMR PLOTS

a)

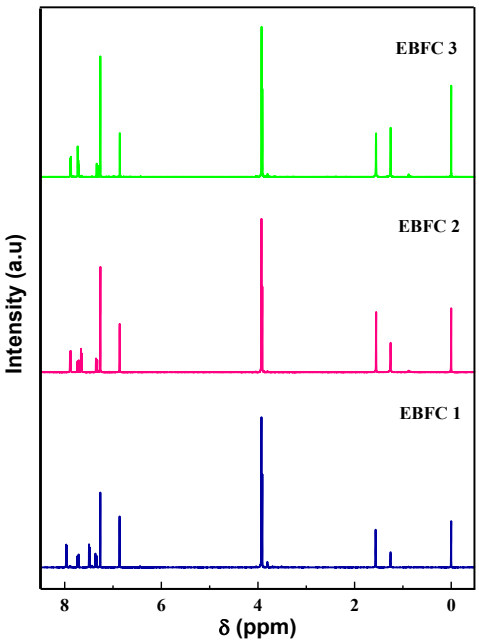

b)

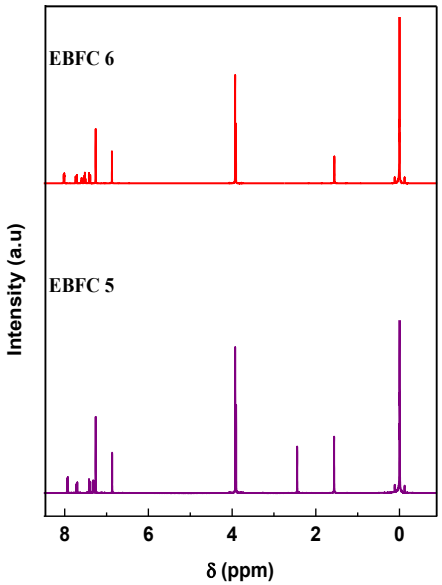

Figure S1. Proton NMR spectra of a) EBFC 1, EBFC 2 and EBFC 3 and b) EBFC 5 and EBFC 6

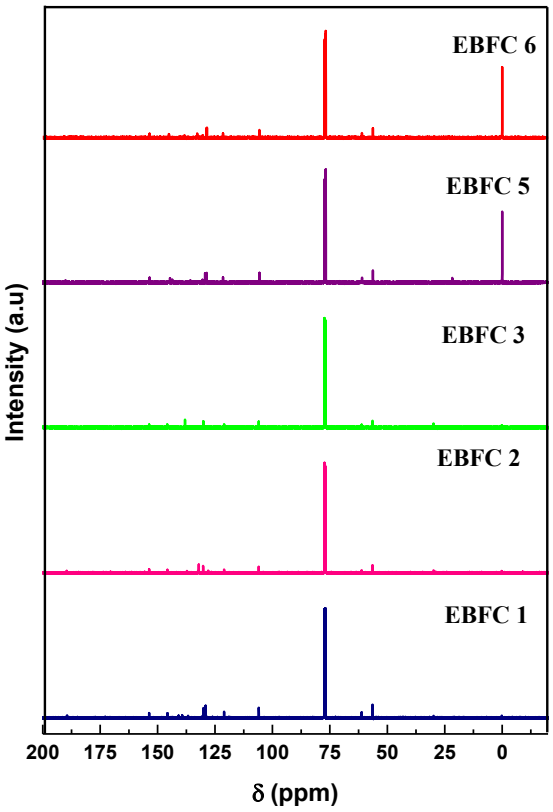

Figure S2. ^{13}C NMR spectra of EBFC 1, EBFC 2, EBFC 3, EBFC 5 and EBFC 6

2. π···π INTERACTIONS AND {110} and {220} PLANES OF UNIT CELL

a)

b)

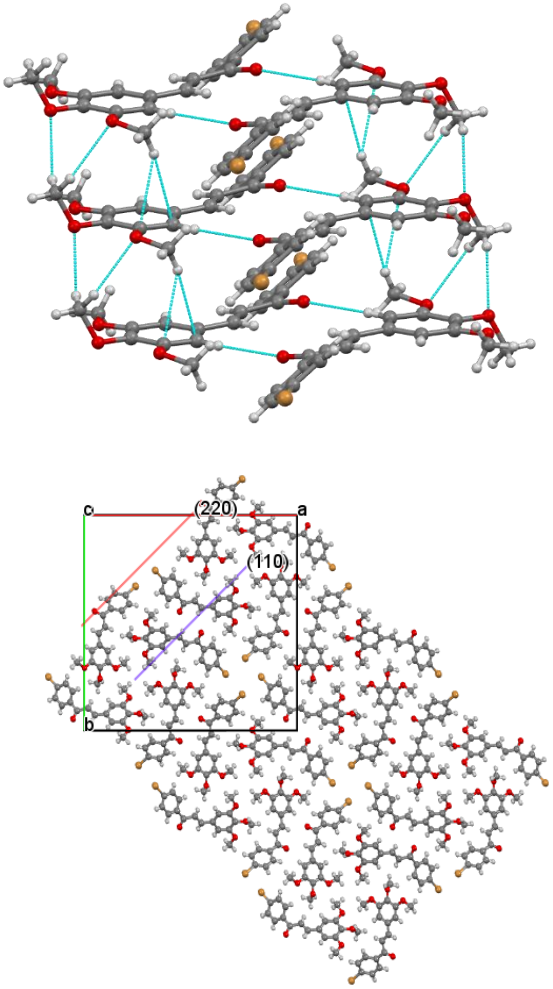

Figure S3. a) π···π interactions and b) {110} and {220} planes of unit cell in EBFC 2

3. Π···Π INTERACTIONS IN EBFC 1 and EBFC 3

a)

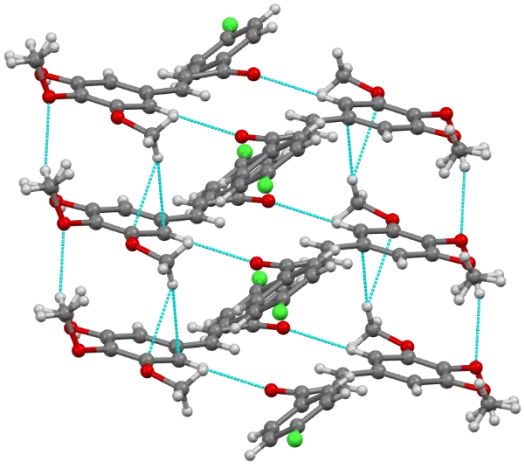

b)

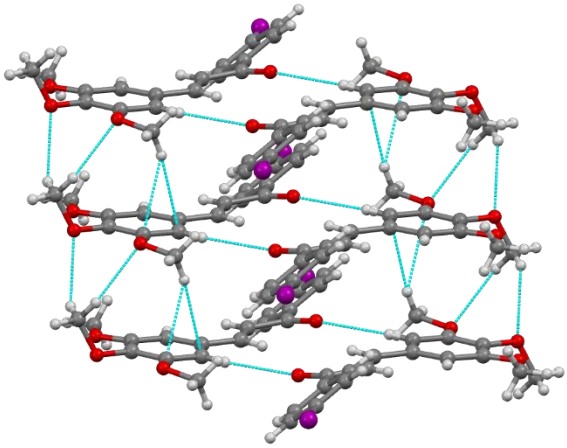

Figure S4. π···π interactions in a) EBFC 1 and b) EBFC 3

4. CRYSTAL PACKING OF EBFC 1 AND EBFC 3

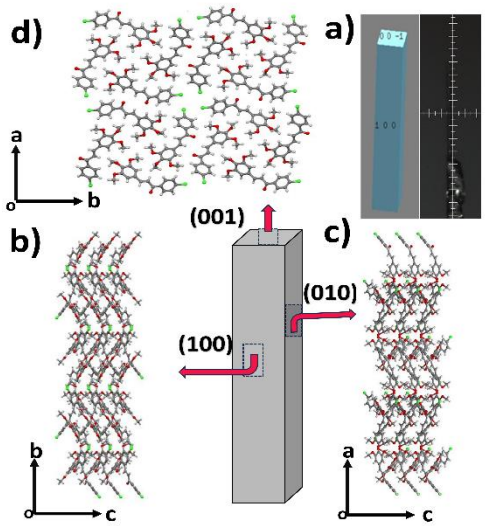

Figure S5. Face indexing image (a) and packing along (b) *a*, (c) *b* and (d) *c* crystallographic axes of EBFC 1

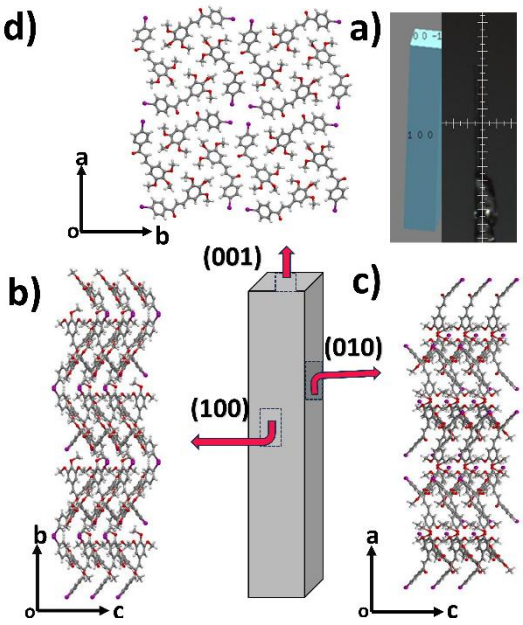

Figure S6. Face indexing image (a) and packing along (b) *a*, (c) *b* and (d) *c* crystallographic axes of EBFC 3

5. CRYSTAL DATA AND STRUCTURE REFINEMENT

Table S1. Crystal data and structure refinement table for EBFC 1, EBFC 2 and EBFC 3

Identification code	EBFC 1	EBFC 2	EBFC 3	EBFC 2A
Empirical formula	C_{18} H_{17} Cl O_4	C_{18} H_{17} Br O_4	C_{18} H_{17} I O_4	C_{18} H_{17} Br O_4
Formula weight	332.76	377.22	424.21	377.22
Temperature	298(2) K	298 K	298(2) K	100(2) K
Wavelength	0.71073	0.71073	0.71073	0.71073
Crystal system	Tetragonal	Tetragonal	Tetragonal	Tetragonal
Space group	P 4_2/n	P 4_2/n	P 4_2/n	P 4_2/n
Unit cell dimensions	a=26.6870(10) Å b=26.6870(10) Å c=4.5014(2) Å α = 90 deg. β = 90 deg. γ = 90 deg.	a = 26.835(4) Å b= 26.835(4) Å c =4.4929(6) Å α = 90 deg. β = 90 deg. γ = 90 deg.	a = 27.221(4) Å b =27.221(4) Å c =4.5059(10) Å α = 90 deg. β = 90 deg. γ = 90 deg.	a = 26.6215(6) Å b = 26.6215(6) Å c=4.42630(10) Å α = 90 deg. β = 90 deg. γ = 90 deg.
Volume	3205.9(3) Å³	3235.4(11) Å³	3338.8(13) Å³	3136.94(16) Å³
Z	8	8	8	8
Calculated density	1.379 gm/cm³	1.549 gm/cm³	1.688 gm/cm³	1.597 gm/cm³
Absorption coefficient	0.256 mm^{-1}	2.559 mm^{-1}	1.935 mm^{-1}	2.639 mm^{-1}
F(000)	1392	1536	1680	1536
Crystal size	0.23 x 0.092 x 0.069	0.15 x 0.07 x 0.05	0.10 x 0.05 x 0.04	0.26 x 0.08 x 0.07

Theta range for data Collection	2.413 to 23.923 deg	2.400 to 32.489 deg.	2.366 to 27.706 deg.	2.164 to 41.229 deg.
Limiting indices	$-34 \leq h \leq 34$, $-34 \leq k \leq 32$, $-5 \leq l \leq 5$	$-31 \leq h \leq 29$, $-31 \leq k \leq 31$, $-5 \leq l \leq 5$	$-34 \leq h \leq 36$, $-36 \leq k \leq 36$ $-6 \leq l \leq 6$	$-49 \leq h \leq 49$, $-49 \leq k \leq 48$, $-8 \leq l \leq 8$
Reflections collected/ unique	38252 / 3562	36822 / 2862	46388 / 4339	93042 / 10458
Refinement method	Full-matrix least-squares on F^2	Full-matrix least-squares on F^2	Full-matrix least-squares on F^2	Full-matrix least-squares on F^2
Data/restraints/ parameters	3562 / 0 / 211	2862 / 0 / 211	4339 / 0 / 211	10458 /0 /211
Goodness-of-fit on F^2	1.062	1.022	1.108	1.06775
Largest diff. peak and hole	0.142 and -0.279 e. A^{-3}	0.265 and -0.343 e. A^{-3}	0.142 and -0.279 e. A^{-3}	0.670 and -0.859 e. A^{-3}
CCDC NO.	2290001	2290002	2290003	2431870

Table S2. Crystal data and structure refinement table for EBFC 5 and EBFC 6

Identification code	EBFC 5	EBFC 6
Empirical formula	$C_{19}H_{20}O_4$	$C_{18}H_{18}O_4$
Formula weight	312.35	298.32
Temperature	298 K	298(2) K
Wavelength	0.71073	0.71073
Crystal system	Orthorhombic	Monoclinic
Space group	Pccn	$P2_1/c$
Unit cell dimensions	a = 19.4274(13) Å b =11.2711(7) Å c =15.5162(11) Å	a= 13.5139(5) Å b= 8.0480(3) Å c =15.0618(5) Å

	α = 90 deg. β = 90 deg. γ = 90 deg.	α = 90 deg. β=109.6760(10) deg. γ = 90 deg.
Volume	3397.6(4) Å^3	1542.47(10) Å^3
Z	8	4
Calculated density	1.221 gm/cm^3	1.285 gm/cm^3
Absorption coefficient	0.085 mm^{-1}	0.090 mm^{-1}
F(000)	1328	632
Crystal size	0.19 x 0.16 x 0.04	0.22 x 0.14 x 0.11
Theta range for data Collection	2.467 to 30.921deg.	2.778 to 25.545deg.
Limiting indices	-23 ≤ h ≤ 23, -13 ≤ k ≤ 13, -18 ≤ l ≤ 18	-19 ≤ h ≤ 19, -11 ≤ k ≤ 11, -21 ≤ l ≤ 21
Reflections collected/ unique	164915 / 3079	99983 / 4565
Refinement method	Full-matrix least-squares on F^2	Full-matrix least-squares on F^2
Data/restraints/ parameters	3079 / 0 / 212	4565 / 0 / 202
Goodness-of-fit on F^2	1.108	1.100
Largest diff. peak and hole	0.184 and -0.179 e. A^{-3}	0.162 and -0.278 e. A^{-3}
CCDC NO.	2479645	2455208

6. TAUC PLOTS AND BAND GAP ENERGY CALCULATION

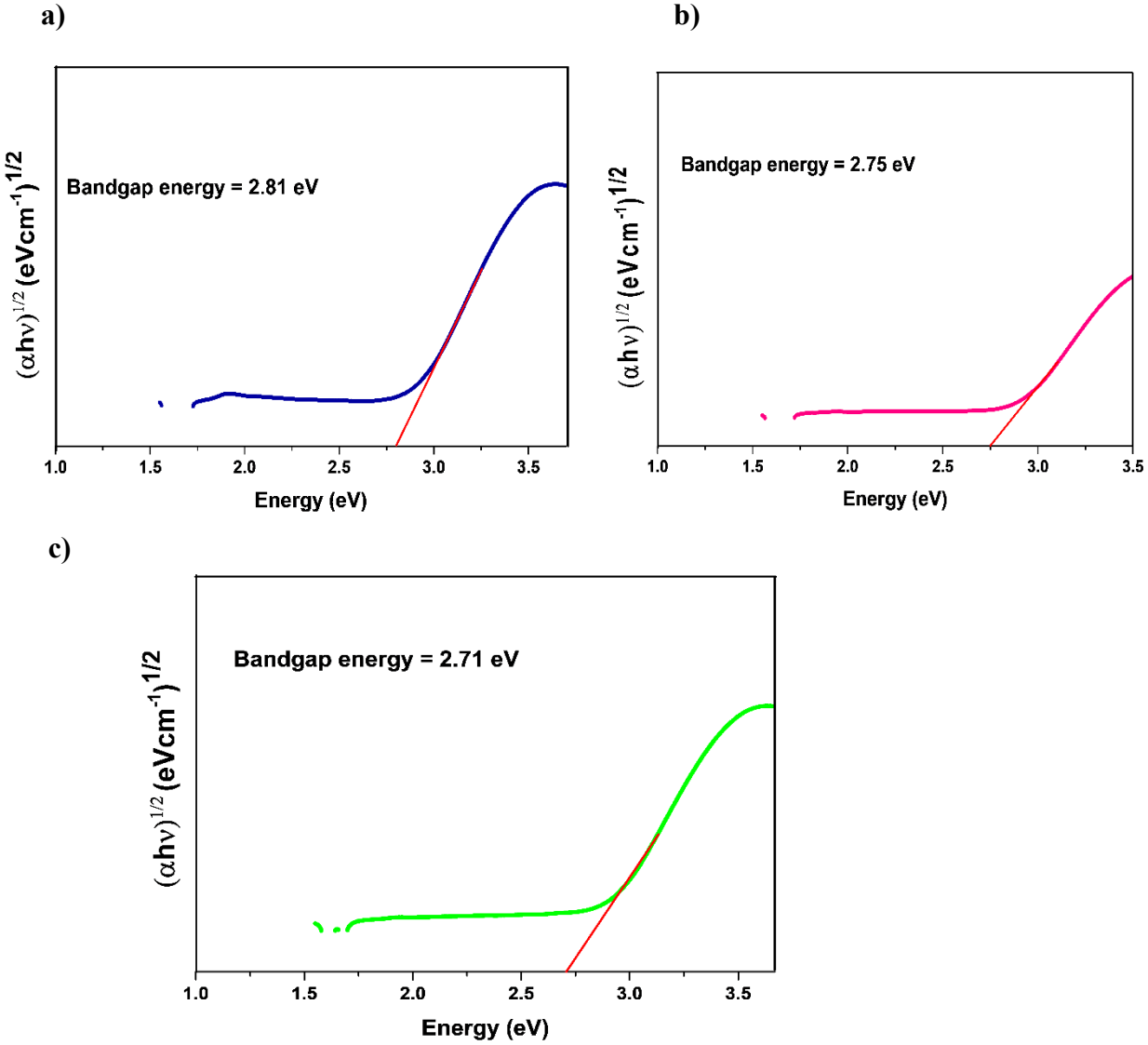

Figure S7. Band gap energy calculation from Tauc plots for a) EBFC 1, b) EBFC 2 and c) EBFC 3

7. MECHANICAL BENDING OF EBFC 1

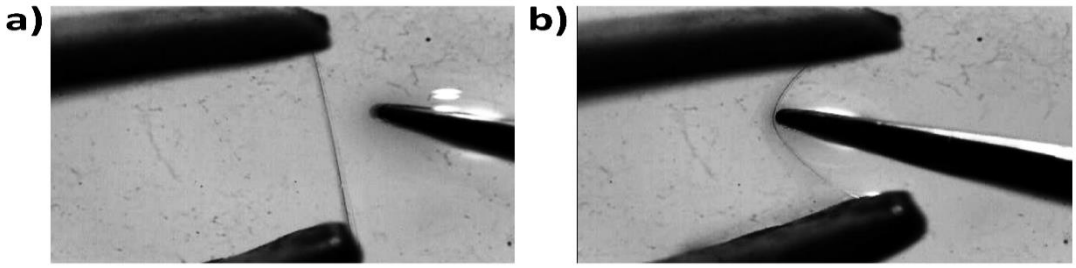

Figure S8. Mechanical bending of EBFC 1

8. INTERMOLECULAR INTERACTIONS

Table S3. Hydrogen bond and tetrel bond geometry (Å, ˚) of EBFC 1

Interaction Type	Bond distance (Å)		Sum of Van der Waal's radii (Å)	Bond Angle (Degree)
	d	*D*		
C—H···O C18—H18···O2 C1—H1B···O1	 2.569 2.617	 3.494 3.372	2.72	 173 135
O—C···O O3—C15···O3	 3.214	 4.628	3.22	 172
C—H···π C17—H17A···C16 C17—H17A···C18	 2.800 2.862	 3.588 3.806	2.90	 167 139

Table S4. Hydrogen-bond and halogen-bond geometry (Å, ˚) of EBFC 3

Interaction Type	Bond distance (Å)	Sum of Van der Waal's radii (Å)		Bond Angle (Degree)
	d	*D*		
C—H···O C15—H15···O4 C1—H1B···O1	 2.664 2.699	 3.579 3.398	2.72	 168 130
C—H···π C16—H16A···C14 C16—H16A···C15	 2.814 2.889	 3.633 3.843	2.90	 143 172
I···I C12—I1···I1	3.854	5.963 4.794	3.96	$\Theta_{1=}$ 177 $\Theta_{2=}$ 103

9. MULLIKKEN NET CHARGE AND MULLIKKEN POPULATION

Table S5. Mullikken net charge in dimer, trimer and tetramer

	Tetrel Bond 1		Tetrel Bond 2		Tetrel Bond 3	
	4 (O)	70 (C)	44 (O)	110 (C)	84 (O)	150 (C)
Dimer	-0.517	-0.231				
Trimer	-0.518	-0.235	-0.523	-0.232		
Tetramer	-0.518	-0.236	-0.525	-0.236	-0.524	-0.232

Table S6. Mullikken population in dimer, trimer and tetramer

	Tetrel Bond 1		Tetrel Bond 2		Tetrel Bond 3	
	4 (O)	70 (C)	44 (O)	110 (C)	84 (O)	150 (C)
Dimer	8.517	6.230				
Trimer	8.517	6.235	8.523	6.215		
Tetramer	8.517	6.236	8.524	6.236	8.524	6.232

10. ORTEP DIAGRAMS OF CHALCONE DERIVATIVES

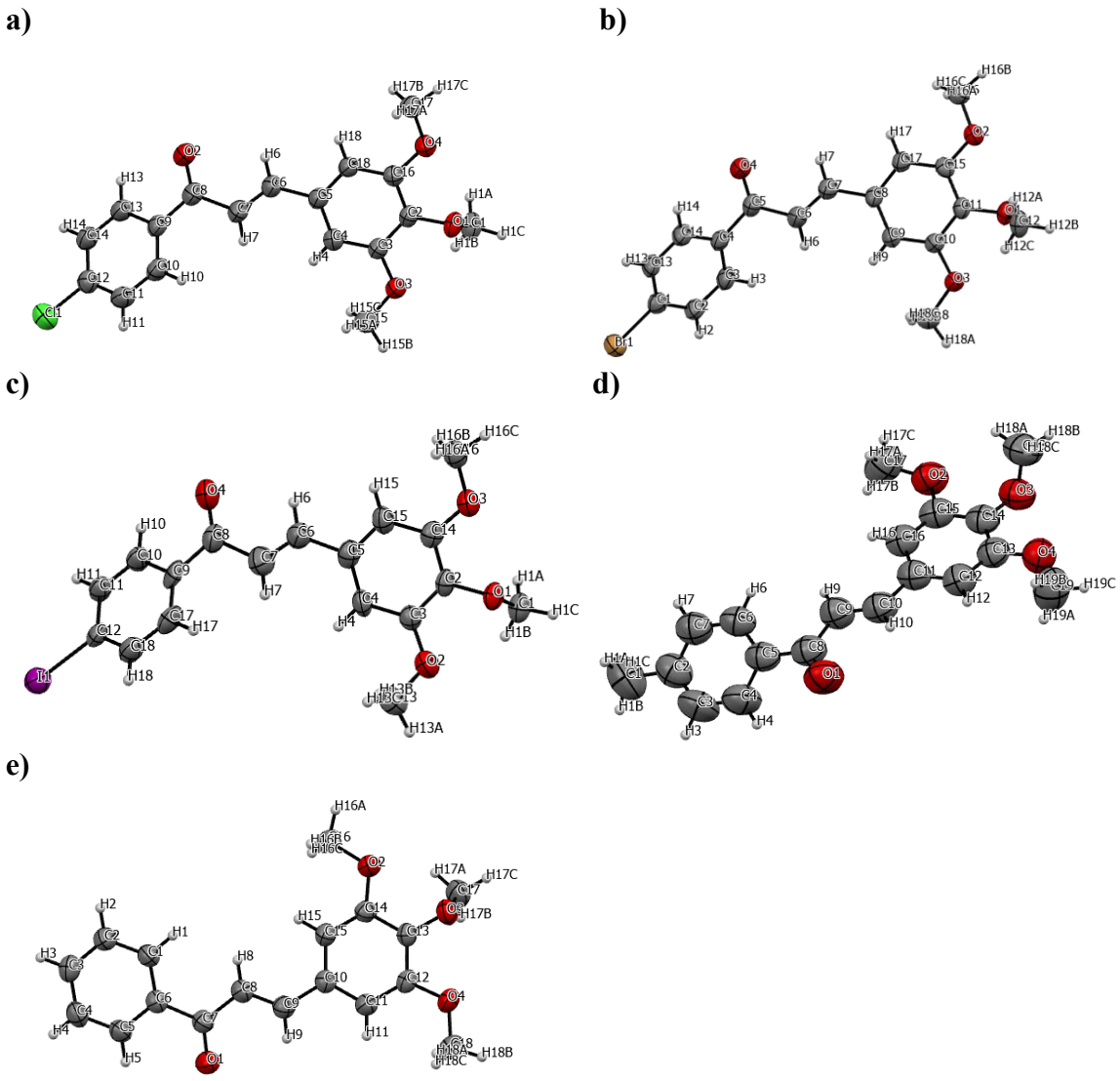

Figure S9. ORTEP diagrams of a) EBFC 1, EBFC 2, EBFC 3, EBFC 5 and EBFC 6

11. CRYSTAL PACKING OF EBFC 5 AND EBFC 6

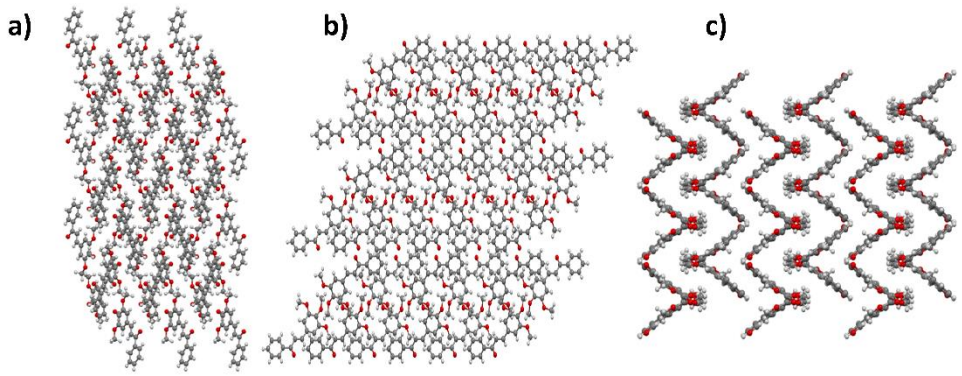

Figure S10. Packing pattern of EBFC 5 along a) *a*, b) *b* and c) *c* crystallographic axes

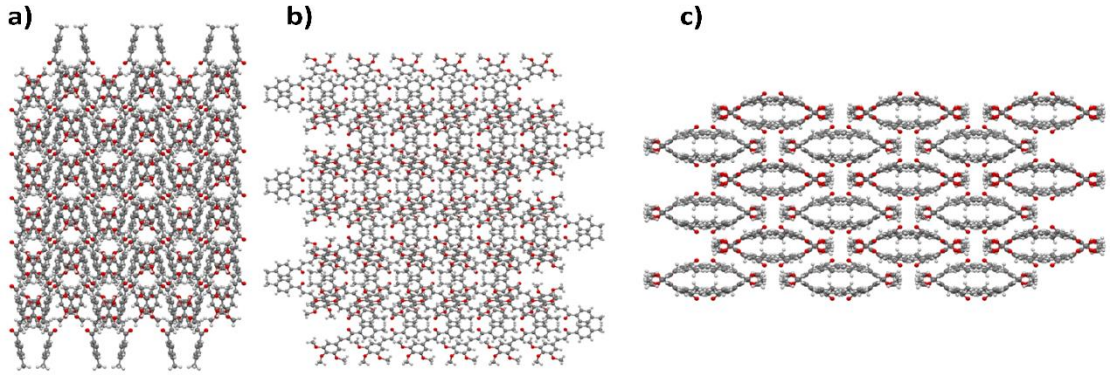

Figure S11. Packing pattern of EBFC 6 along a) *a*, b) *b* and c) *c* crystallographic axes

12. Π···Π INTERACTIONS in EBFC 5 and EBFC 6

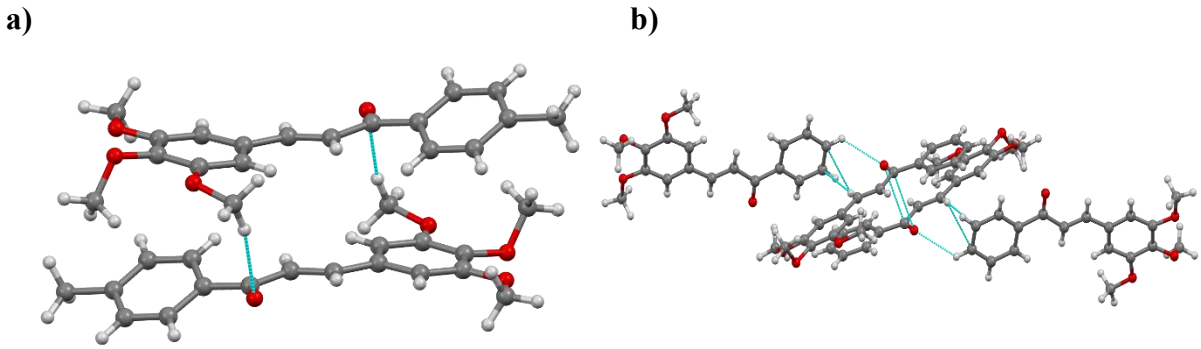

Figure S12. π···π interactions in a) EBFC 5 and b) EBFC 6

13. MECHANICAL BENDING OF EBFC 4

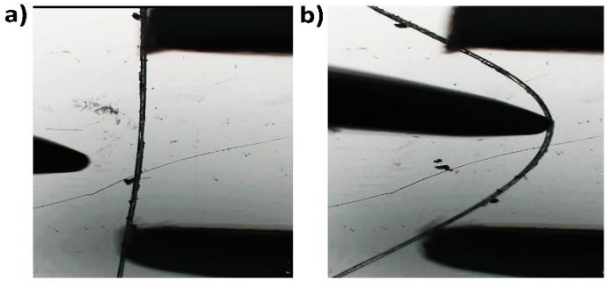

Figure S13. Mechanical bending of EBFC 4

14. THERMAL ANALYSIS

The differential scanning calorimetry (DSC) was carried out with a NETZSCH (DSC 204 F1) instrument at 10 degrees/minute heating rate and the differential thermal analysis (DTA) is carried out with a Netzsch-STA449-F5 simultaneous thermal analyser to find out the melting points of grown crystals (Figure 14 and Figure S14).

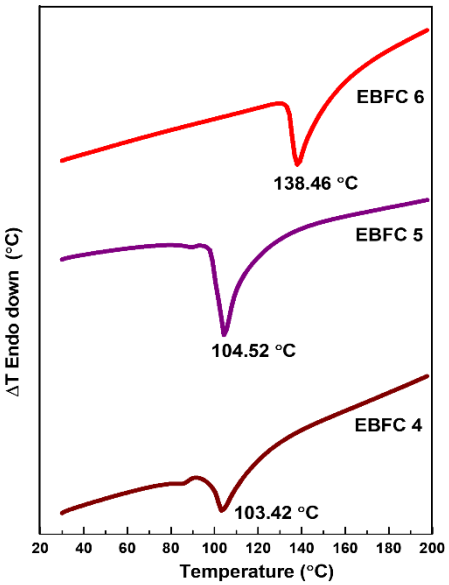

Figure S14. DTA curves of EBFC 4, EBFC 5 and EBFC 6

15. THEORETICAL STUDIES

The investigation proceeded in two stages:

Stage I: Potential Energy Surface Scans: Initial scans were performed by symmetrically varying the C···O tetrel bond distances across the oligomers. This allowed us to map the energy landscape and identify minima corresponding to optimal bond lengths, providing preliminary evidence for cooperativity.

Stage II: Geometry Optimizations: Subsequent full geometry optimizations refined the structures to their energy minima, validating the trends observed in the scans. By comparing bond lengths and interaction energies across dimer, trimer, and tetramer models, we quantified how cooperativity strengthens the tetrel bond with increasing oligomer size.

Potential Energy Surface Scans

Preliminary potential energy scans were performed at the B3LYP/6-31+G(d,p) level of theory. The three C···O tetrel bonds in the tetramer were varied symmetrically and simultaneously in increments of 0.1 Å over a range of 3.0–3.8 Å. The resulting potential energy curves were analyzed to identify energy minima corresponding to optimal tetrel bond lengths. This procedure was repeated for the trimer and dimer by systematically removing one monomer unit from the tetramer and trimer, respectively. The observed gradation in tetrel bond lengths—shortening progressively from dimer (3.32 Å) to tetramer (3.24 Å)—indicated positive cooperativity.

Potential Energy Surface Scanning Methodology

All potential energy surface scans were performed using rigid single-point energy calculations at precisely defined tetrel bond distances:

- Nine discrete C···O tetrel bond distances were sampled: 3.0, 3.1,..., 3.7, 3.8 Å.
- At each distance, single-point energy calculations were performed with completely rigid monomer geometries.
- Only translational movements of entire monomer units were permitted to

achieve the target tetrel bond distances.

- No internal geometry relaxation (bond lengths, angles, or dihedrals) was allowed.
- This discrete sampling approach provides a rigorous energy landscape while maintaining direct comparability with experimental crystallographic data.

Geometry Optimizations

Subsequent geometry optimizations and vibrational frequency calculations were carried out on the dimer, trimer, and tetramer at B3LYP/6-31G(d) level to locate the minimum energy conformations. Convergence criteria included energy thresholds of 10^{-6} Hartree and maximum force thresholds of 0.0003 Hartree/Å. Frequency calculations confirmed the absence of imaginary frequencies, ensuring true minima.

16. X-RAY DIFFRACTION ANALYSIS

The PXRD data are recorded using a Rigaku Miniflex 600 powder X-ray diffractometer within the range of 5˚≥2θ≥50˚ at room temperature. All the peaks exhibited in the PXRD pattern are matched with calculated XRD data obtained from CIF (Figures S15-S18).

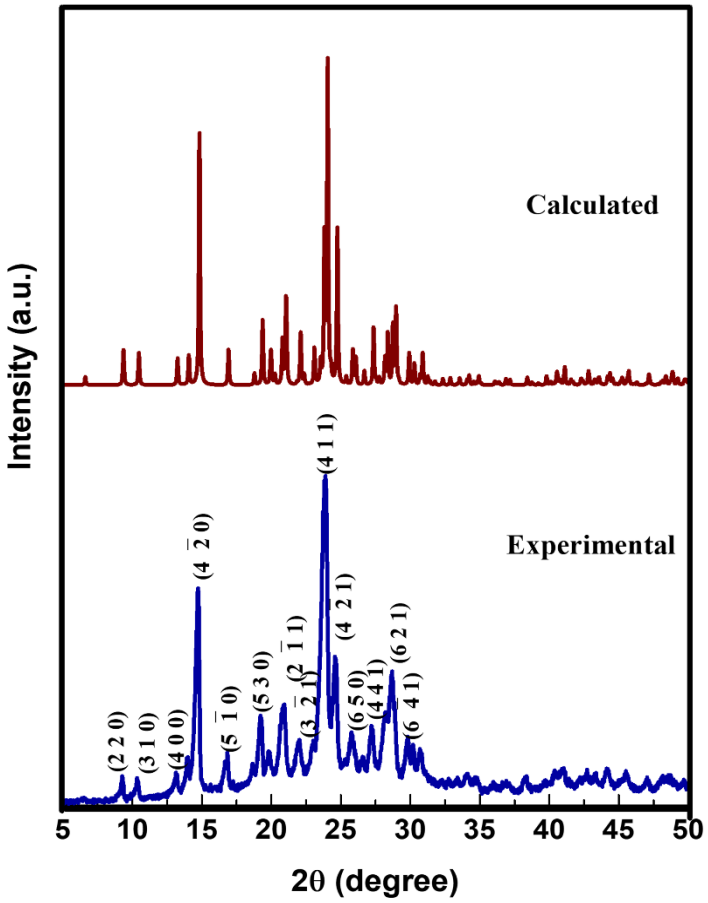

Figure S15. Experimental and calculated PXRD patterns of EBFC 1

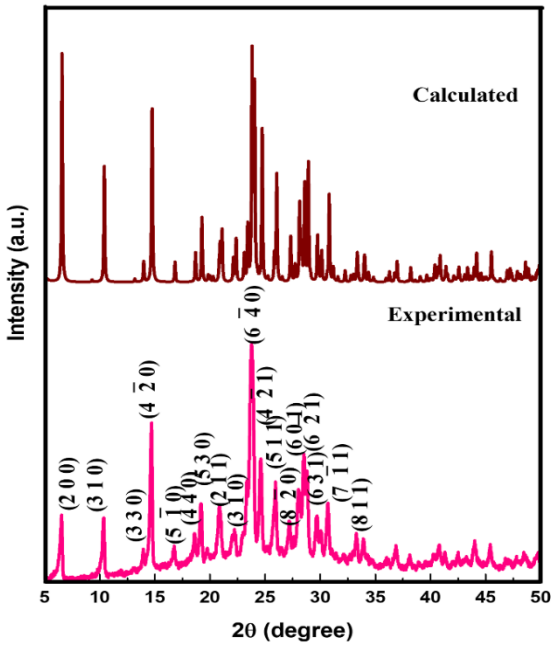

Figure S16. Experimental and calculated PXRD patterns of EBFC 2

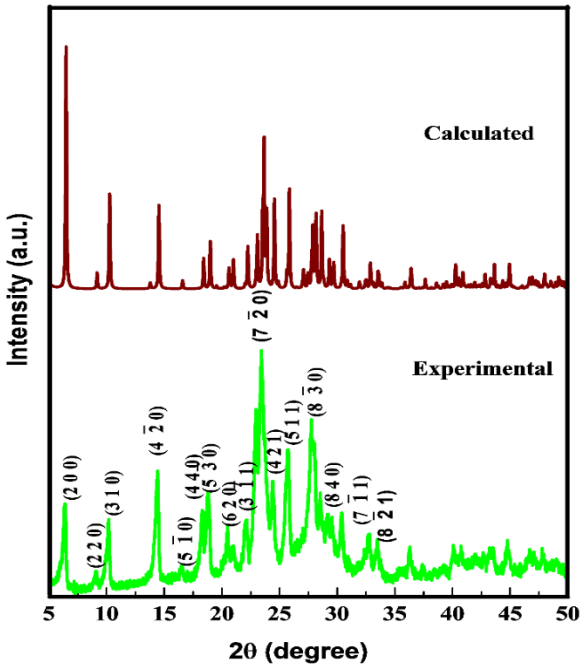

Figure S17. Experimental and calculated PXRD patterns of EBFC 3

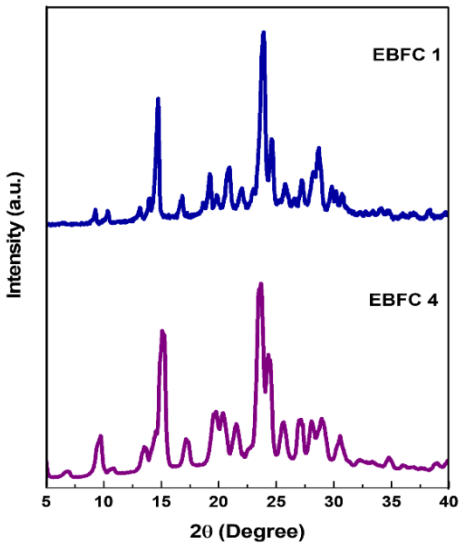

Figure S18. PXRD patterns of EBFC 1 and EBFC 4

17. FT-IR ANALYSIS

The IR spectra of the as synthesised compounds were recorded in the range of 400 cm^{-1} - 4000 cm^{-1} by using an Interspec 200-X FT-IR spectrometer (Figure S19). The different functional groups present were identified and the chemical structures were confirmed. The C-H stretching occurs at 2944 and 2837 cm^{-1}, and carbonyl stretching occurs at 1666 cm^{-1} in EBFC 1. All five crystals exhibit nearly identical frequency values.

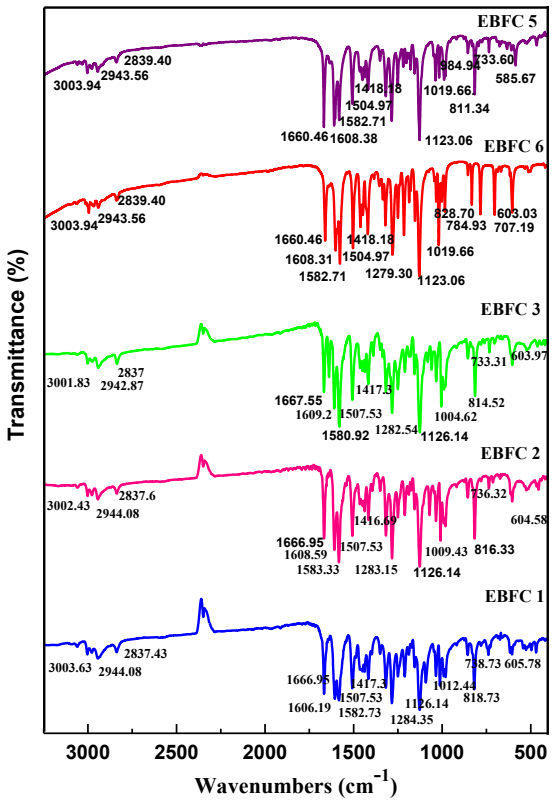

Figure S19. IR plots of EBFC 1, EBFC 2, EBFC 3, EBFC 6 and EBFC 5

18. UV-VISIBLE SPECTROSCOPIC STUDY

The UV-visible spectra are recorded in methanol using JASCO V-660 UV-Visible spectrophotometer with in a wavelength range of 200-800 nm. The absorption takes place in the UV region and the derivatives exhibit wide transparency in the visible region.

19. PHOTOLUMINISCENCE (PL) STUDY

The emission spectra were recorded with a 5-ppm solution in DMSO using Agilent fluorescence spectrophotometer. The excitation wavelength for all three samples is set at 340 nm. The emission spectra were recorded in the wavelength range 400 to 700 nm.

20. LIST OF VIDEOS

Video S1- Mechanical bending of EBFC 2 crystal

Video S2- Mechanical bending of EBFC 1 crystal

Video S3- Mechanical breaking of EBFC 3 crystal

Video S4- Mechanical bending of EBFC 4 crystal